Theoretical Approach to Chebyshev Spectral Collocation Method and Its Mathematical Implementation

Rameshkumar Bhoraniya, Pinank Patel, Ramdevsinh Jhala, and Rajendrasinh Jadeja

Abstract This chapter describes the linear stability investigation of the incompressible viscid flow between the two concentric counter-rotating vertical cylinders. The parallel flow assumption was considered for the base flow, and hence it is varying in the radial direction only. The flow is a shear driven, and hence the pressure gradient is zero in the stream wise direction. The Governing stability equations for the disturbance flow quantities are derived in cylindrical polar coordinates by coupling the energy equation with the Navier-stokes formulas. The stability formulas are discretized using CSC method. The discretized stability formulas, combined with appropriate boundary conditions, form a general Eigenvalues problem (EVP). The full spectrum of the eigenvalue problem is computed for the different Reynolds numbers under the effect of viscous heating, different radius ratio, and buoyancy. The axial and radial wave numbers, β and α are taken as $\pi/2$ and zero, respectively. The effect of viscosity variation due to temperature is introduced by Nahme number (Na) and Brinkman number (Br) and effect of buoyancy by Grashof number (Gr). The acute value of Re of the flow is computed for isothermal and non-isothermal Ta–Co flow including the effect of viscid heating and buoyancy at different radius ratio (η). The viscous heating and buoyancy effect destabilize the flow.

Keywords Stability analysis · Chebyshev · Spectral collocation method · Eigenvalue problem

R. Bhoraniya · P. Patel · R. Jhala · R. Jadeja (✉)
Marwadi University, Rajkot, India
e-mail: rajendrasinh.jadeja@marwadieducation.edu.in

R. Bhoraniya
e-mail: rameshkumar.bhoraniya@marwadieduction.edu.in

P. Patel
e-mail: pinank.patel@marwadieduction.edu.in

R. Jhala
e-mail: ramdevsinh.jhala@marwadieducation.edu.in

Nomenclature

T	Temperature
μ	Viscosity
ρ	Density
C_p	Specific Heat
d	Diameter of Cylinder
g	Gravitational Acceleration
η	Radius Ratio
Pr	Prandtl number
Gr	Grashof number
Re	Reynold's Number
R_{cr}	Critical Reynolds number
Na	Nahme Number
Br	Brinkmen Number
α	Azimuthal wave number
β	Axial wave number

Abbreviations

ODE	Ordinary Differential Equation
PDE	Partial Differential Equation
EVP	Eigenvalue Problem
FDM	Finite Difference MethodFinite Difference Method (FDM)
FEM	Finite element MethodsFinite Element Method (FEM)
CSC	Chebyshev Spectral Collocation
Ta–Co	Taylor–Couette flow

1 Introduction

The (PDEs) and its applications are important in the field of applied mathematics. These are a basic form of equations in the number of applications of physics, natural science and finance. They are used to describe the local properties of the function in the three-dimensional fluid flow problems.

The concept of discretization is the easiest set of rules to approximate the solution of PDEs. In this process, the PDEs are represented as the determinate dimensional problem. At the same time, replacing the Partial differential equation by a distinct model is not insignificant at all, and more often, the choice of the determinate dimensional model to be used depends on the properties behind the mathematical model

itself. The Recent advances in computer technologies have made it easier to determine accurate solutions of the PDEs efficiently, even in the most critical cases of very large systems of PDEs.

The FDM and FEM methods are often used for the mathematical solution of PDEs. However, in the computations of the spatial derivatives, these methods essentially require a massive number of nodal points to provide an accurate numerical solution. The Spectral and Pseudo-spectral methods have been developed as an alternative solution to it in recent years. The spectral methods are different from the FDM and FEM methods, in spectral methods global information is integrated in the calculation of a spatial derivative. The spectral methods can provide greater accuracy for a smooth solution with the use of a very less number of nodes and, therefore, less calculation time as compared to FDM and FEM.

The spectral procedures are widely used for the flow simulations due to higher accuracy. However, it is very difficult to apply it to complex geometries, and generally, it is used for simple geometries. The method of collocation is a numerical solution method for the ODE, PDE and integral equations. In the collocation method, a finite-dimensional space of solution is chosen (most often polynomials), and a number of collocation points are also chosen. Then a solution is selected such that it fulfills the condition of a given equations at the association positions. The orthogonal collocation on finite elements is also used to solve a PDE from Fluid Dynamics. Association locations are selected as the roots of orthogonal polynomials gave better results because of a few striking characteristics of these polynomials.

The main objective of the authors is to study the Spectral collocation method using Chebyshev polynomial and to demonstrate its application for the numerical solution of fluid flow problem. The stability examination of the incompressible flow passing between the two rotating cylinders having same axis of rotation (Ta–Co flow) has been carried out to demonstrate the application of Spectral collocation method. Sections 1 and 2 presents basic introduction, mathematical background and relevant literature review. The governing stability equations, boundary conditions and numerical solution of then eigenvalue problem is discussed in Sect. 3. Section 4 presents solution of base flow temperature profile under the effect of variable viscosity. The validation of the computed results and effect of radius ratio, viscous heating and bouncy on the stability of Ta–Co flow have been discussed in the Sects. 5 and 6.

2 Chebyshev Method

The CSC method is used in discretizing the governing equations and group more grid point at the boundary of a domain. The CSC Method is Global in Nature. In this method Computation at any point depends on information from whole domain. The Chebyshev Spectral Collocation Method provides exponential Convergence rate. This method provides precise results with moderate number of grid points.

Let us consider one ODE, $y'(t) = f(t, (y(t)), y(t_0) = y_0$ The equation is required to be resolved in the interim $[t_0, t_0 + C_k h]$. Choose C_k from $0 \leq c_1 < c_2 < \cdots < c_n \leq 1$. The compliant polynomial association method come close to the result y by the polynomial p of degree n this solution contents the primary condition $qt(0) = y_0$, it also satisfies the variance equation

$$q'(t_0 + h) = f(t_0 + h, q(t_0 + h))$$
$$y_1 = q(t_0 + h)$$

$q'(t_m) = f(t_m, q(t_m))$ at all association points $t_m = (t_0 + C_m h)$ for $m = 1, 2, \ldots$ n. This results in $n + 1$ conditions, which equals the $n + 1$ constraints needed to identify a polynomial of degree n. The association methods used here are implied "Runge Kutta methods". The constants C_m in the "Butcher stand of a Runge Kutta method" are the association points. It may be important to understand that not all implied Runge–Kutta methods are association methods. The association method can be explained with following case. Let us consider two association points $C_1 = 0$ and $C_2 = 1$.

The association conditions are

$$qt(0) = y_0 \tag{1}$$

$$q' = f(t_0, q(t_0)) \tag{2}$$

$$q'(t_0 + h) = f(t_0 + h, q(t_0 + h)). \tag{3}$$

Above mentioned three conditions are used in collocation method, this indicates that p has to be a polynomial of second degree. We can also write the function q as: $q(t) = \alpha(t - t_0)^2 + \beta(t - t_0) + \gamma$ this will help us to reduce the calculations. The coefficients are evaluated by using collocation conditions.

$$\alpha = \frac{1}{2h} = f((t_0 + h, q(t_0 + h) - f(t_0, q_0)), \beta = f(t_0, p_0), \gamma = y_0 \tag{4}$$
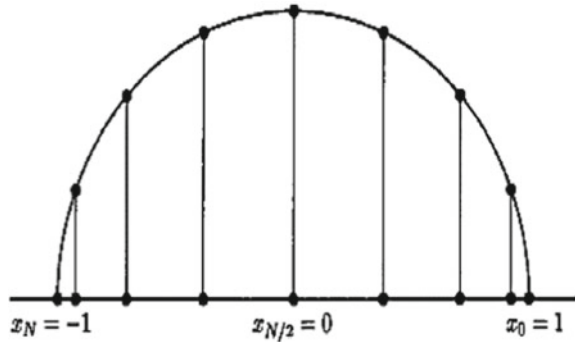
The collocation method is now given by

$$y_1 = q(t_0 + h) = y_0 + \frac{1}{2}h(f(t_0 + h), y_1) + f(t_0, y_0)) \tag{5}$$

where, $y_1 = q(t_0 + h)$ is approximate solution at $t = (t_0 + h)$.

The Chebyshev method is used to calculate number of collocation points in a domain. Following figure shows the distribution of collocation points in the given domain.

Fig. 1 Chebyshev point distribution

It is evident from the Fig. 1 that Chebyshev locations are placed at equal distance on to the upper half of the unit circle but its projection on to the x-axis are not equally spaced. There are more grid locations which are present at the extreme points in comparison with the center or we can say that there is clustering of grid points at the extreme points in comparison with to the center, it is also observed that the space between grid points at ends is less in comparison to space between grid points at the center so there is finer mesh at the boundary, which will help to have better and accurate results. CSC methods support to characterize a function in best possible way with the help of few representative points.

Periodic Function: The sample points which are evenly spaced throughout the interval are selected to describe a periodic function over an interval. These sample points are selected using N function samples, and they form a trigonometric inter-pellant comprising of a sum of N sinusoids. This methodology produces merger in N for integration, differentiation, and interpolation.

Non-periodic functions: A Non-periodic function over an interval is characterized with the help of N function examples, the interval is mapped into $[-1, 1]$. The sample points are chosen based on Chebyshev criteria and a polynomial interplant comprising of a sum of N Chebyshev polynomials is created by the selected points. This method offers convergence exponential in N for integration, differentiation, and interpolation.

Comparison of the Chebyshev Spectral Collocation Method with Analytical Method:
The comparison of CSC Methods is done by using derivative of the Sin (X) with the help of analytical method as well as by CSC method.

The Square in the Fig. 2 represents the results using Analytical Method and star represents the results using spectral method. The results depict that the CSC method provides closely accurate to analytical solution points.

Chebyshev differentiation:
If a vector f_{even} is trajectory of function models considered at equally spaced points in an interval [a, b] i.e. if
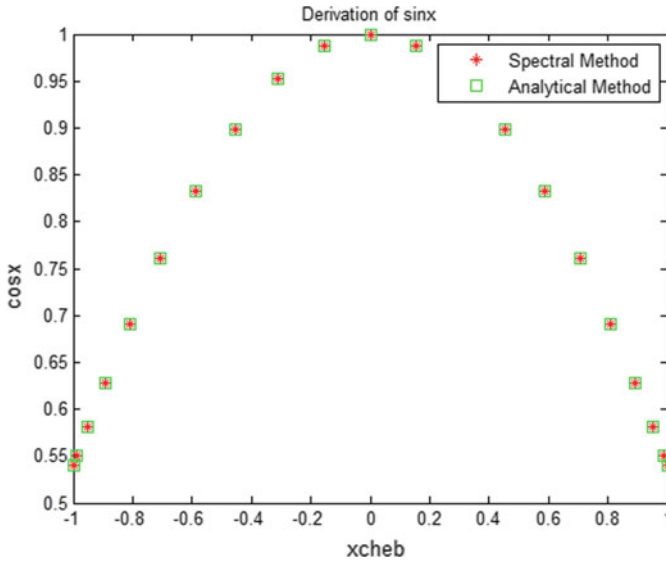
Fig. 2 CSC and analytical method results

$$f_{even} = \begin{pmatrix} f(a) \\ f(a + \Delta) \\ f(a + 2\Delta \\ . \\ . \\ f(b) \end{pmatrix} \tag{6}$$

Then, the vector of derived values at choose points can be presented in the form of a centered FDM calculation it will be in the form of a matrix vector product of $f'_{even} = D^{CFD}$

Where,

$$D^{CFD} = \frac{1}{2\Delta} \begin{pmatrix} 0 & 1 & 0 & 0 \cdots 0 & 0 \\ -1 & 0 & 1 & 0 \cdots 0 & 0 \\ 0 & -1 & 0 & 1 \cdots 0 & 0 \\ 0 & 0 & -1 & 0 \cdots 0 & 0 \\ \vdots & \vdots & \vdots & \vdots \vdots & \vdots & \vdots \\ 0 & 0 & 0 & 0 & 0 & 0 & 1 \\ 0 & 0 & 0 & 0 & 0 & -1 & 0 \end{pmatrix} \tag{7}$$

This approximation will converge like $1/N^2$. In Chebyshev spectral method we just need to construct the Nth Chebyshev approximant $\int_{approx}(x)$) to f(x) and differentiate the variable of approximation and considering this as an approximation to the

derivative. The Nth Chebyshev approximation to f(x) is

$$\int_{approx}(x) = \sum_{m=0}^{N} C_m T_m(x) \tag{8}$$

Differentiating we get

$$f\prime_{approx}(x) = \sum_{m=0}^{N} C_m T\prime_m(x) \tag{9}$$

Now when we calculate the results of this equation at the (N + 1) Chebyshev points: $X_n = \cos\frac{n\pi}{X}$ Where n = 1, 2, … N, we achieve vector $f\prime_{cheb}$. The entries of this vector are estimated values of the derivative of f_{cheb} at the Chebyshev points, and it is related to the vector C of Chebyshev coefficients via a matrix-vector product relationship:

$$N_{Gn} = \frac{\mu_0 U_\infty^2}{k\Delta T_0}; \text{R}_e = \frac{\rho U_\infty d}{\mu}; P_r = \frac{\mu_0 C_p}{k}; G_r = \frac{g\rho^2\beta\Delta T_0 d^3}{\mu_0^2} \tag{10}$$

$f'_{cheb} = T'C$ where T' is (N + 1) x(N + 1) dimensional Matrix.

If we consider the relation C = Λf_{cheb} We receive $f\prime_{cheb}$ = T'Λf_{cheb} where $Dcheb = T'\Lambda$ matrix that functions on a vector of models at Chebyshev points to produce a vector of f_0 samples at Chebyshev points.

2.1 Application of Spectral Collocation Method in Fluid Dynamic Problems

The bounded flows through channels and other simple geometries are simple in configurations. However, they are too important from the scientific and technological aspects. The vortices generated at corners and in the flow direction, flow transition, and turbulence can be analyzed in the same bounded configurations. To study two-dimensional and three-dimensional flow problems, one can use an arithmetical result of the Na-S equations. The primitive variable and vortices-Stream function approached are used to study viscous fluid flow problems. In the first variable approach, a coupling of pressure and velocity is challenging to satisfy the incompressibility condition.

In the case of a vortices-stream function approach, such a problem, the pressure term is eliminated from the equations. However, the order of the derivative increases in this formulation. In a two-dimensional fluid flow problem, this approach is widely used. However, a straight forward extension of it for three-dimensional flow is not that

easy due to the increased order of derivatives. Thus, the primitive variable approach is more suitable for 3D problems [1].

The non-iterative methods like estimate method and small step method have been developed to prevent the coupling of pressure-velocity difficulty of the primitive variable approach. In the methods mentioned above, no special memory storage is required, and they are suitable for the solution of unsteady flow problems. These methods use the prediction-correction method in which pressure is predicted from the projected velocity in the divergence-free velocity field.

The higher-order temporal scheme with the spectral method is used to improve accuracy by incorporating a variation of the projection method with the pseudo-spectral method. A semi-implicit projection system with second-order accuracy in temporal discretization gives good numerical stability in spectral collocation form. The diagonalization is performed, which is an effective and efficient direct method of solution. This combination of a temporal scheme with spectral-spatial discretization is giving a very fast solution in comparison to the iterative solution procedure. The combination of the two higher order of accurate methods has been validated using square opening flow at Re = 10,000 and backward-facing step in channel flow at Re = 875 [1].

Taylor–Couette flow is a drag driven flow in which flow is produced by the relative circular motion of the cylinders. Therefore, the outside compelling by a pressure gradient is not present [2]. It is an ideal case for studying the flow instability of Newtonian and Viscoelastic fluids. Couette and Mallock are the first to investigate the stability analysis of the viscous incompressible flow [3]. The first mathematical representation of the flow between two concentric, infinite long cylinders having rotary motion in three dimensions was successfully developed by G. I. Taylor and obtained a result that was similar to the experimental results [4]. The work started by Taylor continues the study of two-dimensional flow between the cylinders, which is Taylor's classical problem [5]. There are many theories available to analyze the stability of the flow i.e. energy gradient theory, classical linear theory, Non-linear theory, etc. The majority of the study has been performed on the steadiness of Ta- Co flow without viscid heating effect. Ali and Weidman (1990) theoretically investigated the effect of the temperature gradient in the radial direction on the volatility of the Ta–Co flow [6].

They show that for a given Prandtl number (Pr), the subordinate flow is symmetrical about the axis, and the perilous value of Re surges with the increase in Gr. The resilience force has a steadying result except for large value Pr number fluids. However, the subordinate flow becomes asymmetric about the axis for larger Gr, and Rcr number decreases with increasing Gr [7]. Kolyshkin and Vaillancourt (1993) studied effect of energetics on isothermal Ta–Co flow for a radius ratio from 0.4 to 0.95 and Pr from 1 to 100. They found that the disturbances which are symmetric about an axis are most hazardous turbulences, and flow is disrupted as Pr and Gr increases [8]. The thermal buoyancy effect on the instability was examined by Dah-Chyi Kuo and K. S. Ball (1997). The critical value of Re for the finite annulus is almost equal to the forecast based on linear stability results for continuous length for the isothermal case. The Rcr number for non-isothermal flow is slightly less as compared

to that of isothermal Ta–Co flow [9]. The majority of the research is performed on the steadiness of the Couette flow with the rotary motion of either inside or outside cylinder or with motion about the axis of the inner cylinder depending upon the application [10]. The stability of the channel flow, pipe flow, Couette, and boundary layer flow with viscous heating has been examined by several authors [11, 12]. The experiment of the stability isothermal Ta–Co flow with viscid heating of Newtonian fluid has been studied by White and Mullar [13]. They admitted that the uncertainty of flow is resulted due to a connection between viscid indulgence encouraged temperature stratification and inertial forces. In the case of viscous heating of the fluid, the property viscosity is used the temperature-dependent, and Nahme type viscosity-temperature rise is used to analyze the effect of temperature on the viscosity. Al-Mubaiyedh, Sureshkumar & Khomami (1999) per-formed instability analysis to analyze the effect of viscid indulgence on the Ta–Co flow instability. They considered liquids of high viscidness and large initiation energy with temperature-dependent viscosity [14]. Na provides the degree of thermal compassion of the fluid. Al-Mubaiyedh et al. (2002) studied in detail the thermal influence on the distribution of pressure and kinematics also uneven disturbances to know the flow disruption mechanism due to viscid heating [15]. They predicted a new mode of instability due to viscous heating effect in the absence of buoyancy effect with higher Pr (11000). At high Pr as Na increases, the coupling between radial disturbances and temperature gradient enhances centrifugal instability [16]. In the case of the instability of the Ta–Co flow, the effects of non-isothermal are the result of viscid indulgence and not because of a forced temperature gradient, which has not been studied significantly [17, 18]. In this chapter, we have presented the study of the effect of viscid heating and buoyancy on the stability characteristics of the Ta–Co flow for different radius ratios of the cylinders with uniform i.e., isothermal and non-uniform wall heating i.e., Non-isothermal.

3   Problem Formulation

The incompressible and Newtonian fluid with viscous heating is considered among two concentric rotating cylinders. The walls of the cylinder are kept at the same temperature in the matter of isothermal Ta–Co flow and different invariable temperatures for non-isothermal Taylor–Couette flow. The governing stability equations (Linearized Navier-Stoke equations) are derived using the standard procedure. The space between the two rotating cylinders is very small in comparison to the radii of the inside cylinder. The Reynolds number based on the spaced $= (R_2 - R_1)/2)$ between inside and outside cylinder is considered, where R_1 and R_2 are the inside and outside radii of the cylinder, respectively. The radius of the cylinders is normalized by the gap (d). The base flow is changing in the radial direction only. However, the disturbances are three dimensional. Both the cylinders are rotating in opposite directions with the same angular velocity. Viscid indulgence is encompassed in the energy equation through generation number (NGn), which is described as the maximum change of temperature due to viscid heating regulated by the controlled wall temperature,

which is known as Nahme number (Na) and Brinkman number (Br) for isothermal and non-isothermal Taylor–Couette flow respectively [6]. The following relation is used to determine the variation of viscosity with the change in temperature [19].

$$\mu = \mu_0 \exp\left[\beta \frac{T - T_0}{T_0}\right] \tag{11}$$

μ_0 is the reference viscidness at temperature T_0 and it is a non-dimensional initiation energy parameter that characterize the change in viscosity with reference to temperature variation; where β is a positive number for the liquids. The Generation number (N_{Gn}), Reynolds Number (Re), Prandtl number (Pr) and Grashof number (Gr) are defined as,

$$N_{Gn} = \frac{\mu_0 U_\infty^2}{k \Delta T_0}; R_e = \frac{\rho U_\infty d}{\mu}; P_r = \frac{\mu_0 C_p}{k}; G_r = \frac{g\rho^2 \beta \Delta T_0 d^3}{\mu_0^2} \tag{12}$$

where, ΔT_0 is the reference temperature difference, β is thermal expansion co-effcient at reference temperature T_0. The disturbances are assumed to be in normal mode form with the amplitudes are the functions of a radial coordinate only

$$\overline{U_r} = 0 + u_r; \overline{U}_\theta = U_\theta + \mu_\theta; \overline{U}_z = 0 + u_z; \overline{P} = P + p; \overline{\mu} = \mu + \mu' \tag{13}$$

$$q(r, t) = \hat{q}(r)e^{[i(\alpha\theta + \beta Z - \omega t)]} \tag{14}$$

where q $= [u_r, \mu_\theta, \mu_\phi, P]$, $\overline{Q} = [\overline{Ur, U\theta, U\phi, P}]$, r is radial coordinate, z is axial coordinate, θ is azimuth coordinate, ω is circular frequency, α is azimuth wave number, and β is axial wave number.

$$\frac{\partial u}{\partial r} + \frac{U_\theta}{r}\frac{\partial u_r}{\partial \theta} - \frac{2U_\theta}{r}u_\theta = -\frac{\partial P}{\partial r} + \frac{1}{R_e}\begin{bmatrix} 2\mu\frac{\partial^2 u_r}{\partial^2 r} + 2\frac{\partial u}{\partial r}\frac{\partial u_r}{\partial r} + 2\frac{\mu}{r}\frac{\partial^2 u_r}{\partial^2 r} + \\ \frac{\mu}{r}\left(\frac{\partial u_\theta}{\partial_r \partial\theta} - \frac{1}{r}\frac{\partial u_\theta}{\partial\theta} + \frac{1}{r2}\frac{\partial^2 u_r}{\partial^2\theta}\right) + \\ \frac{1}{r}\frac{\mu}{\theta}\left(\frac{\partial u_\theta}{\partial r}\frac{u_\theta}{r}\right) - 2\frac{\mu}{r^2}\left(\frac{\partial u_\theta}{\partial\theta} + u_r\right) + \\ \left(\mu\left(\frac{\partial^2 u_z}{\partial r \partial z} + \frac{\partial^2 u_r}{\partial z^2}\right)\right) - \frac{G_r}{R_e^2}T \end{bmatrix} \tag{15}$$

$$\frac{\partial u_\theta}{\partial t} + \left(\frac{\partial u_\theta}{\partial r} + \frac{u_\theta}{r}\right)u_r + \frac{u_\theta}{r}\frac{\partial u_\theta}{\partial r} = -\frac{1}{r}\frac{\partial P}{\partial\theta} + \frac{1}{R_e}$$

$$\left[\begin{array}{c} \dfrac{\partial u}{\partial r}\left(\dfrac{\partial u_\theta}{\partial r} - \dfrac{u_\theta}{r} + \dfrac{1}{r}\dfrac{\partial u_r}{\partial \theta}\right) + \mu \left(\begin{array}{c} \dfrac{\partial^2 u_\theta}{\partial r^2} - \dfrac{1}{r}\dfrac{\partial u_\theta}{\partial r} + \dfrac{u_\theta}{r^2} \\[2mm] + \dfrac{1}{r}\dfrac{\partial^2 u_r}{\partial \theta \partial r} - \dfrac{1}{r^2}\dfrac{\partial u_r}{\partial \theta} \end{array}\right) + \\[4mm] \mu \left(\dfrac{\partial u_\theta}{\partial r^2} + \dfrac{u_\theta}{r^2} - \dfrac{1}{r}\dfrac{\partial u_\theta}{\partial r}\right) + \dfrac{2\mu}{r}\left(\dfrac{2}{r}\dfrac{\partial u_r}{\partial \theta} - \dfrac{u_\theta}{r} + \dfrac{\partial u_\theta}{\partial r} + \dfrac{1}{r}\dfrac{\partial^2 u_\theta}{\partial \theta^2}\right) \\[4mm] + \dfrac{2\mu}{r}\left(\dfrac{u_\theta}{\partial r} - \dfrac{u_\theta}{r}\right) + \mu \left(\dfrac{\partial u_\theta}{\partial z^2} + \dfrac{\partial^2 u_z}{\partial \theta_z}\right) \end{array}\right] \tag{16}$$

$$\dfrac{\partial u_z}{\partial t} + \dfrac{u_\theta}{r}\dfrac{\partial u_z}{\partial \theta} = \dfrac{\partial P}{\partial \theta} + \dfrac{1}{R_e}\left[\begin{array}{c} \dfrac{\partial u}{\partial r}\left(\dfrac{\partial u_z}{\partial r} + \dfrac{\partial u_r}{\partial z}\right) + \mu \left(\dfrac{\partial^2 u_z}{\partial r^2} + \dfrac{\partial^2 u_z}{\partial z \partial r}\right) + \\[3mm] \dfrac{\mu}{r}\left(\dfrac{\partial u_z}{\partial r} + \dfrac{\partial u_r}{\partial z}\right) - \dfrac{Gr}{Re^2}T \end{array}\right] \tag{17}$$

$$\dfrac{\partial T}{\partial t} + u_r \dfrac{\partial T}{\partial r} + \dfrac{u_\theta}{r}\dfrac{\partial T}{\partial \theta} + u_z \dfrac{\partial T}{\partial z} = \dfrac{1}{R_e P_r}\dfrac{\partial^2 T}{\partial r^2} + \dfrac{1}{r}\dfrac{\partial T}{\partial r} + \dfrac{1}{r^2}\dfrac{\partial^2 T}{\partial \theta^2} + \dfrac{\partial^2 T}{\partial z^2} +$$
$$\dfrac{N_{Gn}}{R_e P_r}\mu \left(\dfrac{\partial u_\theta}{\partial r} - \dfrac{u_\theta}{r}\right)\dfrac{\partial u_\theta}{\partial r} - \dfrac{1}{r}\left(\dfrac{\partial u_\theta}{\partial r} - \dfrac{u_\theta}{r}\right) \tag{18}$$

$$\dfrac{\partial u_r}{\partial r} + \dfrac{u_r}{r} + \dfrac{1}{r}\dfrac{\partial u_\theta}{\partial \theta} + \dfrac{\partial u_z}{\partial_z} \tag{19}$$

3.1 Boundary Conditions

At inside and outside wall of the cylinders, the boundary conditions assumed are that there is no slip and there is no penetration for each disturbance velocity components. At the wall, all disturbance velocity components are zero. Another boundary condition taken into account is that at wall pressure do not exists.

$$u_r = (x, r_{out}) = 0; \; u_0 = (x, t_{out}) = 0; \; u_z = (x, r_{out}) = 0 \tag{20}$$

$$u_r = (x, r_{out}) = 0; \; u_0 = (x, t_{out}) = 0; \; u_z = (x, r_{out}) = 0 \tag{21}$$

Though, the compatibility regulations resulted from the Linearized N-S equations have been collocated at the solid wall.

$$\dfrac{1}{R}\left[2\overline{\mu}\dfrac{\partial^2 u_r}{\partial r^2} + 2\dfrac{\partial \overline{u}}{\partial_r}\dfrac{\partial u_r}{\partial r} + \dfrac{2\overline{u}}{r}\dfrac{\partial u_r}{\partial_r}\right] - \dfrac{1}{R_e}\left[\dfrac{i\alpha \overline{u}}{r}\dfrac{\partial u_\theta}{\partial_r}\right] - \dfrac{1}{R_e}\left[i\beta \overline{u}\dfrac{\partial u_\theta}{\partial_r}\right] + \dfrac{\partial P}{\partial r} \tag{22}$$

The CSC technique is used to discretize the governing stability equations [17]. This discretization makes the non-uniform nature of the distribution of the grid points with a greater number of grids towards the end. For boundary value problems, it is a favorable arrangement.

$$r_{cheb} = \cos\left(\frac{\pi i}{n}\right) \text{ where i = 1, 2, 3 ... n} \tag{23}$$

where n = Total number of collocation points.

The stability equations together with the boundary conditions forms a general EVP of the form,

$$
\begin{bmatrix}
A_{11} & A_{12} & A_{13} & A_{14} & A_{15} \\
A_{21} & A_{22} & A_{23} & A_{24} & A_{25} \\
A_{31} & A_{32} & A_{33} & A_{34} & A_{35} \\
A_{41} & A_{42} & A_{43} & A_{44} & A_{45} \\
A_{51} & A_{52} & A_{53} & A_{54} & A_{55}
\end{bmatrix}
\begin{bmatrix} u_r \\ u_\theta \\ u_z \\ p \\ T \end{bmatrix}
= i\omega
\begin{bmatrix}
B_{11} & B_{12} & B_{13} & B_{14} & B_{15} \\
B_{21} & B_{22} & B_{23} & B_{24} & B_{25} \\
B_{31} & B_{32} & B_{33} & B_{34} & B_{35} \\
B_{41} & B_{42} & B_{43} & B_{44} & B_{45} \\
B_{51} & B_{52} & B_{53} & B_{54} & B_{55}
\end{bmatrix}
\begin{bmatrix} u_r \\ u_\theta \\ u_z \\ p \\ T \end{bmatrix}
\tag{24}
$$

$$[A][\phi] = i\omega[B][\phi] \tag{25}$$

where, A and B are real matrices of size 5 × n , iω is an eigenvalue and φ is the eigenvector. The QZ algorithm is employed for the solution of the EVP.

4 Base Flow Solution

The fully-developed steady and parallel incompressible base flow is considered between the concentric rotating cylinders in opposite directions. The base is varying along the radial direction only. The thermal stratification is also considered in the radial direction. Thus, the viscosity is varying and it is dependent on the temperature of the fluid. The energy equation is coupled with the Navier-Stokes equation and the reduced non-dimensional equations for the base flow are as follow,

$$\frac{1}{r}\frac{\partial}{\partial r}\left(r\frac{\partial T}{\partial r}\right) + N_{Gn}\mu\left[r\frac{\partial}{\partial r}\left(\frac{U_\theta}{r}\right)\right]^2 = 0 \tag{26}$$

$$\frac{1}{r}\frac{\partial}{\partial r}\left(r\frac{\partial T}{\partial r}\right) + N_{Gn}\mu\left[r\frac{\partial}{\partial r}\left(\frac{U_\theta}{r}\right)\right]^2 = 0 \tag{27}$$

The conditions (28) and (29) are co nsidered for the solution of above equations.

$$u_\theta(x, r_{in}) = +1, \; T(x, r_{in}) = r_{t1} \tag{28}$$

$$u_\theta(x, r_{out}) = -1, \ T(x, r_{out}) = r_{t_2}; \ \text{where} \ r_{t_1} = \frac{T_1 - T_0}{\Delta T_0}; \ r_{t_2} = \frac{T_2 - T_0}{\Delta T_0} \quad (29)$$

Stream wise (azimuth) velocity, temperature and viscosity respectively. The base flow equations for constant viscosity are simple and solved analytically and it is not presented here because the variation in the base flow velocity profile is very small. The Eqs. 28 and 29 are solved with the help of series solution up to second order accuracy [6, 15].

Figure 3a shows the effect of non-dimensional temperature (r_t) on the temperature profile of the flow. The $r_t = 0$ is the isothermal flow in which the inside and outside cylinder ramparts are maintained at equal temperature. Figure 1b presents the temperature profile for various values of Na. It shows that the increase in Na, increases the variation in temperature. The escalation in Brinkman number (Br) also surges the temperature variation for non-isothermal flow.

5 Code Validation

The results obtained for the present computations are compared with the results of P. Schmid and L. Tuckerman (2002) for $\eta = 0.5$ and $\eta = 0.99$ without viscid heating effect. The azimuthal (α) and axial (β) wave numbers are 0 and $\pi/2$. The eigen spectrum shown in Fig. 2a, b are very similar to the results of Schmid et al. [18]. Thus, the code is validated against the results of P. Schmid et al. (2002) (Fig. 4).

6 Results and Discussions

In the present stability analysis, two cylinders are revolving in contrary directions, and hence the speed ratio Ω_1 is as -1. The range of different values of η is changing from 0.5 to 0.99. The radial length and the velocities are controlled by the space, d $= (R_2 - R_1)$ and $\Omega_1 R_1$ respectively. The magnitude of α and β are zero and unity respectively. The stability analysis for the Ta–Co flow is with the variable viscosity due to the viscous heating effect. The generation numbers like Nehme (Na) number and Brinkman (Br) numbers are defined to incorporate the variation of viscosity and temperature on the steadiness representative of the Ta–Co flow.

6.1 Effect of Radius Ratio (η)

In the case of the adiabatic wall conditions, the fluid viscosity remains constant. The Eigenvalues problem is solved to compute the least stable Eigenvalue and associated

Fig. 3 Effect of
a temperature (r_t), **b** Nahme
number (Na) and **c** Brinkman
number (Br) on temperature
profile for radius ratio $\eta =$
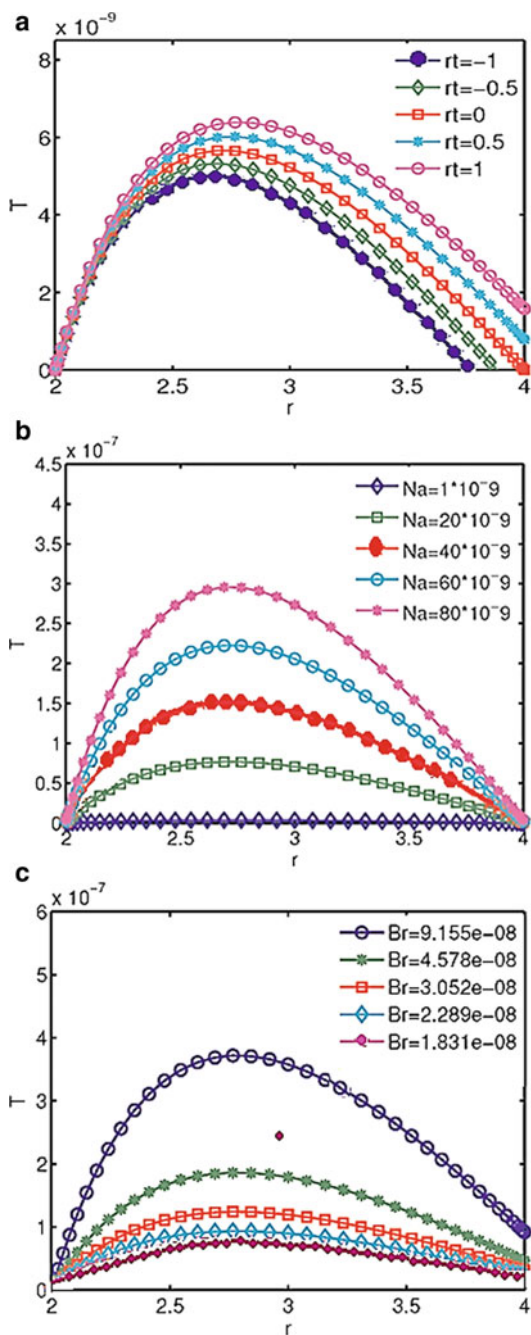0.5 speed ratio $\frac{\Omega_1}{\Omega_2} = -1$

Fig. 4 Eigen spectrum for
a $\eta = 0{:}5$ and Re $= 125$ **b** η
$= 0{:}99$ and Re $= 350$. The
α, β and speed ratio are 0, $\frac{\pi}{2}$
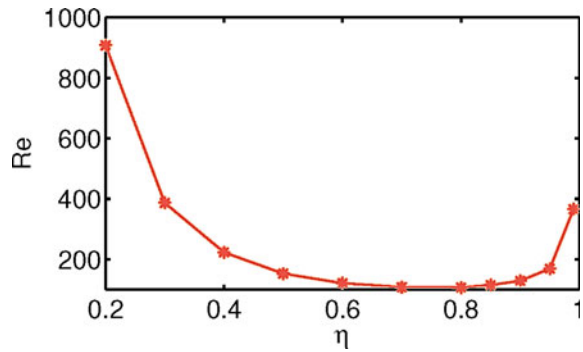and -1
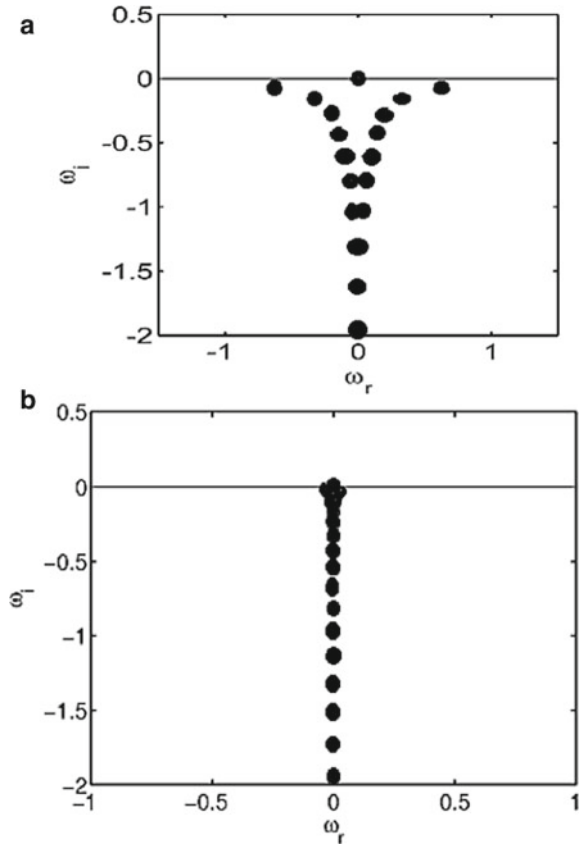
Fig. 5 Effect of radius ratio
η on the R_{cr}

Eigenfunctions for different values of η. The perilous value of Re is determined for
the range of various values of radius ratio.

Figure 5 shows the change in the value of the critical Reynolds number for different radius ratio η. It shows that R_{cr} number reduces as η increases from 0.2 to 0.7, it is nearly constant in the range of η 0.7 to 0.8 and beyond 0.8 it increases.

6.2 Effect of Viscous Heating

To study the viscid heating effect on the instability characteristic of Ta–Co flow, two different cases are considered. In the first case, the inside and outside boundaries of the cylinders are maintained at a fixed temperature of 25 °C, and so it is called isothermal Ta–Co flow. The viscosity of the fluid is variable due to the heating effect. The R_{cr} number is computed for η = 0.5 and η = 0.99.

Table 1 shows the assessment of the critical value of Re for η = 0.5 and η = 0.99 for adiabatic and isothermal wall conditions of the rotating cylinders. The critical value of Re is lower for isothermal Ta–Co flow compared to adiabatic wall of the cylinders. This indicates that Taylor–Couette flow becomes unstable with the viscous heating effect at a lower Reynolds number.

Figure 6 shows the change in the value of critical Re for different Nahme numbers. Na introduces the viscous heat dissipation. The increase in the speed of rotation increases the heat dissipation effect. The Na number is varied by increasing the rotating speed of the wall of both the cylinders. It has been found that the critical value of Re reduces with the rise in Na Number. Thus, the increase in Nahme number has destabilizing effect on the Taylor–Couette flow. Table 2 shows a comparison of R_{cr} number for isothermal Ta–Co flow for η = 0.5 and η = 0.99. It shows that the R_{cr} number reduces with the viscid heating effect. This, in turn, proves that viscous heating has a destabilization effect on the disturbances. In the second case, the inside and outside walls of the cylinders are maintained at different values of constant temperature. The temperature gradient is present in the radial direction. The viscous heating effect is introduced in this case using Brinkman's number. The Brinkman number reduces with the increase in temperature difference of cylinder walls. The variation of critical R_e against Br is shown in Fig. 4b. It shows that the critical value of R_e raised with the rise in the value of Br. Thus, an increase in the Brinkman number stabilizes the flow. Table 3 shows the critical value of Re for different values of $\Delta T0$ for non-isothermal Taylor–Couette flow. It shows that as the ΔT_0 rises, the critical value of Re decreases. It is also witnessed that the critical R_e for non-isothermal Taylor–Couette flow is smaller than that of isothermal Taylor–Couette flow.

Table 1 Assessment of the R_{cr} for isothermal Ta–Co flow

Radius ratio	Critical R_{cr_1}	Critical R_{cr_2}
0.5	153	130
0.99	366	312

Fig. 6 Effect of **a** Nahme number, Na and **b** Brinkman man number, Br on the R_{cr} number for $\eta = 0{:}5$ and speed ratio $\frac{\Omega_1}{\Omega_2} = -1$
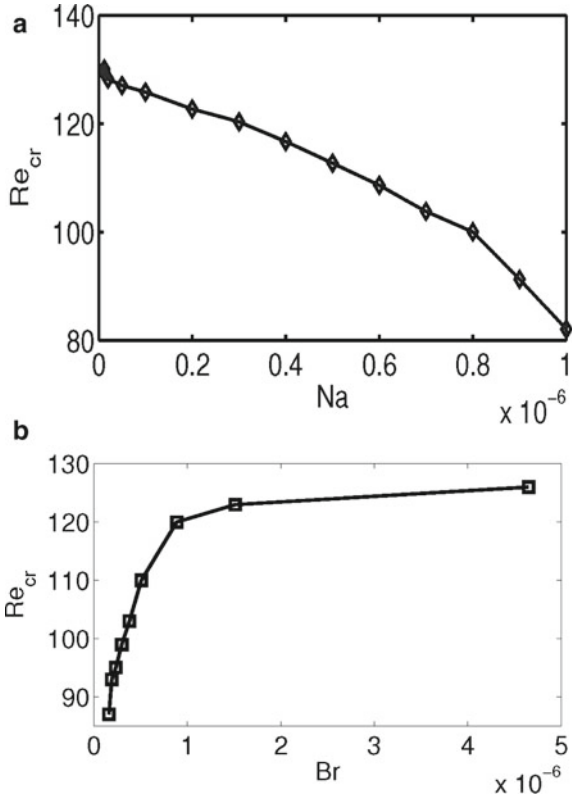

Table 2 Assessment of Rcr number for isothermal Ta–Co flow with buoyancy effect

Radius ratio	Critical R_{cr_1}	Critical R_{cr_2}
0.5	130	128
0.99	312	310

Table 3 Comparison of R_{cr} number for non-isothermal Ta–Co flow with buoyancy effect. Here ΔT_0 is the temperature difference of walls of inner and outer cylinders

Radius ratio		Critical R_{e1}	Critical R_{e2}
0.5	−0.2	131	128
	0.5	120	118
	1.0	103	100
0.99	−0.2	320	310
	0.5	304	300
	1.0	296	292

Fig. 7 Variation of Rcr
number versus temperature
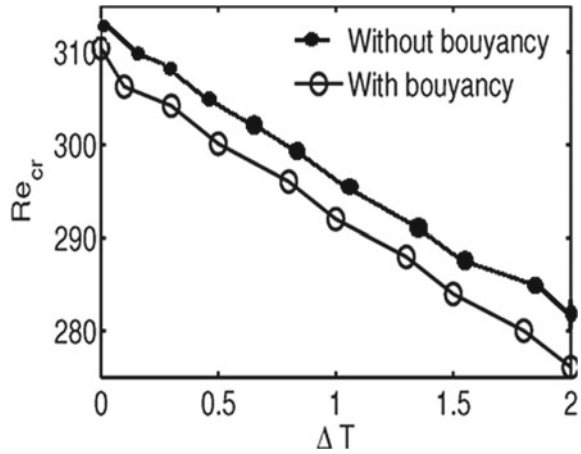
6.3   Effect of Buoyancy

The effect of buoyancy is studied for isothermal and non-isothermal Ta–Co flow. The effect of buoyancy is combined in the governing equations using Gr number.

From the above results, we observe that in isothermal Ta–Co flow with buoyancy, with the increase in radius ratio from 0.5 to 0.99 there is an increase in R_{cr}.

Figure 7 shows the variation of the Rcr number with the reference temperature difference. It is found that the buoyancy effect reduces the critical Re for the same temperature difference for $\eta = 0.5$ and $\eta = 0.99$.

7   Conclusions

The local temporal Eigenmodes are computed using linear stability theory for Ta–Co flow. The effect of viscid heating and buoyancy are studied on the steadiness characteristics of Ta–Co flow. To study the effect of viscid heating for isothermal and non-isothermal Taylor–Couette flow Nahme and Brinkman numbers are introduced. The general Eigenvalue problem is solved to determine the least stable Eigenmode. For adiabatic wall conditions, it is found that the critical value of Re reduces with the increase in radius ratio up to $\eta = 0.8$, beyond which critical value of Re increases. The isothermal and non-isothermal Taylor–Couette flow is studied by introducing generation number like Nahme and Brinkman number. The critical value of Re increases with the rise in Nahme number while reduces with the increase in Brinkman number. The critical value of Re reduces with the increase in the temperature difference of cylinder walls. It is also observed that the flow becomes unstable at a lower Reynolds

number in case of a non-isothermal flow. The critical value of Re with the buoyancy effect is found smaller for isothermal and non-isothermal. Thus, buoyancy has a stabilizing effect on the disturbances.

References

1. Martinez JJ et al (2007) A Chebyshev collocation spectral method for numerical simulation of incompressible flow problems. J Braz Soc Mech Sci Eng
2. Thomas DG (2004) Thermo-mechanical instabilities in Dean and Taylor–Couette flows mechanisms and scaling laws. J Fluid Mech
3. Drazin P, Raid WH (2004) Hydrodynamic stability. Cambridge University Press. https://doi.org/10.1017/CBO9780511616938
4. Taylor GI (1923) The spectrum of turbulence. Roy Soc London, Ser Math Phys Sci 223:289
5. Belotserkovskii OM, Oparin AM et al (2016) Coherent hydrodynamic structures and vortex dynamics. Math Model Comput Simuls, Math Phys 135–148
6. White JM, Muller SJ (2002) Experimental studies on the stability of Newtonian Taylor–Couette flow in the presence of viscous heating. J Fluid Mech
7. Ali M, Weidman PD (1990) On the stability of circular Couette flow with radial heating. J Fluid Mech 53:220
8. Kolyshkin AA, Vaillancourt R (1997) Convective instability boundary of Couette flow between rotating porous cylinders with axial and radial flows. Phys Fluids 5:3136
9. Kuo DC, Ball KS (1997) Taylor–Couette flow with buoyancy: Onset of spiral flow. Phys Fluids 9:2872
10. Renardy Y, Joseph D (1985) Couette flow of two fluids between concentric cylinders. J Fluid Mech 150:381
11. Mosta S, Sinbanda P (2010) A novel numerical technique for two-dimensional laminar flow between two moving porous walls. In: Mathematical problems in engineering Hindawi Publication
12. Papathanasion TD (1968) Thermomechanical coupling in frictionally heated circular Couette flow. Int J Thermo-Phys 18:825
13. White M, Mullar J (2000) Viscous heating and the stability of newtonian and viscoelastic taylor–couette flows. Am Phys Soc 84:5130
14. Al-Mubaiyedh UA, Sureshkumar R (1999) Influence of energetics on the stability of viscoelastic Taylor–Couette flow. Phys Fluids 11:3217
15. Al-Mubaiyedh UA, Sureshkumar R et al (2002) The effect of viscous heating on the stability of Taylor–Couette flow. J Fluid Mech 46:111
16. Dou H, Khoo B, Yeo K (2008) Instability of Taylor–Couette flow between concentric rotating cylinders. Int J Therm Sci 46:262
17. Johnny de Jesús Martinez (2007) A Chebyshev collocation spectral method for numerical simulation of incompressible flow problems. J Braz Soc Mech Sci Eng 29:3
18. Schmid P, Tuckerman L (2002) Transient growth in Taylor–Couette flow. Phys Fluids 14:3474
19. White JM (2000) Viscous heating and the stability of newtonian and viscoelastic Taylor–Couette flows. Phys Rev Lett